

Linear analysis and crossphase dynamics in the ∇T_e -driven CTEM fluid model

M. Leconte¹, Lei Qi¹ and J. Anderson²

¹ Korea Institute of Fusion Energy (KFE), Daejeon 34133, South Korea

² Department of Space, Earth and Environment Sciences,
Chalmers University of Technology, SE-412 96 Göteborg, Sweden

E-mail: mleconte@kfe.re.kr

January 2, 2023

Abstract

Collisionless trapped-electron mode (CTEM) turbulence is an important contributor to heat and particle transport in fusion devices. The ITG/TEM fluid models are rarely treated analytically, due to the large number of transport channels involved, e.g. particle and ion/electron heat transport. The ∇T_e -driven CTEM fluid model [Anderson et al, *Plasma Phys. Control. Fusion* 48, 651 (2006)] provides a simplified model, in the regime where the density gradient drive is negligible compared to the electron temperature gradient drive (∇T_e). This provides an interesting model to study mechanisms associated to linear waves, such as crossphase dynamics, and its possible role in the formation of $E \times B$ staircase. Here, the ∇T_e -driven CTEM fluid model is rigorously derived from the more general ITG/TEM model, and its linear dynamics is first analyzed and compared with CTEM gyrokinetic simulations with bounce-averaged kinetic electrons, while nonlinear analysis is left for future work. Comparisons of linear ITG spectrum are also made with other analytical models.

1 Introduction

In magnetic fusion devices, electron heat transport and particle transport is partly due to collisionless trapped-electron mode (CTEM) turbulence, which is usually coupled to ion-temperature gradient (ITG) turbulence. The CTEM is an instability due to the toroidal precession-drift resonance of trapped electrons in the low-collisionality regime [1]. It is driven by electron temperature gradient and/or density gradient. The Chalmers model [2, 3, 4, 5, 6] provides a simple yet predictive set of fluid models for ITG and CTEM turbulence. This set of models has been analyzed linearly. However, there remain certain aspects which are not fully understood, such as the crossphase dynamics responsible for the transport [7, 8, 9, 10]. In this article, we first analyze the ITG-TEM model linearly - including the crossphase dynamics. Focusing on the limit of ∇T_e -driven CTEM, the two-field model of Ref. [6] is analyzed further and compared to linear gyrokinetic simulations with bounce-averaged kinetic electrons [11]. The future goal is to analyze zonal electron temperature corrugations associated to zonal staircase with nonlinear simulations [12, 13, 14], its relation to zonal flows, and its possible relation to the transport crossphase [7, 8]. This is left for future work.

The rest of this article is organized as follows. In Section 2, we present the general ITG-TEM model used in this study, a linear analysis and general crossphase dynamics analysis is presented. The derivation of the ITG dispersion relation is reviewed and compared to linear gyrokinetic simulations. In section 3, we focus on the ∇T_e -driven CTEM, a subset of the ITG-TEM model. The model is analyzed - including the detailed crossphase dynamics - and compared with linear gyrokinetic simulations. In section 4, we discuss the results and present conclusions.

2 Model

We are interested in collisionless trapped electron modes (CTEM) for which the frequency verifies $k_{\parallel}v_{th,i} \ll \omega_k < k_y v_{th,e}$. Although electron trapping is a toroidal phenomenon, we assume a slab geometry, for simplicity. We consider the following fluid model of collisionless trapped-electron mode turbulence,

based on Nordman et al. [3]:

$$\frac{\partial n}{\partial t} + \mathbf{v}_E \cdot \nabla n + f_t v_{*e} \frac{\partial \phi}{\partial y} = -\epsilon_n g_e v_{*e} \frac{\partial}{\partial y} (n - f_t \phi + f_t T_{et}), \quad (1)$$

$$\frac{\partial T_{et}}{\partial t} + \mathbf{v}_E \cdot \nabla T_{et} + \eta_e v_{*e} \frac{\partial \phi}{\partial y} = -\frac{\Gamma - 1}{f_t} \epsilon_n g_e v_{*e} \frac{\partial}{\partial y} \left(n - f_t \phi + (1 + \frac{\Gamma}{\Gamma - 1}) f_t T_{et} \right), \quad (2)$$

$$\left[\frac{\partial}{\partial t} + \mathbf{v}_E \cdot \nabla \right] \left[(1 - f_t) \tilde{\phi} - \nabla_{\perp}^2 \phi \right] + (1 - f_t + \frac{1 + \eta_i}{\tau} \nabla_{\perp}^2) v_{*e} \frac{\partial \phi}{\partial y} = \epsilon_n g_i v_{*e} \frac{\partial}{\partial y} \left[(1 - f_t) (g_e/g_i + 1/\tau) \phi + T_i + (g_e/g_i + 1/\tau) n + (g_e/g_i) f_t T_{et} \right], \quad (3)$$

$$\begin{aligned} \frac{\partial T_i}{\partial t} + \mathbf{v}_E \cdot \nabla T_i &= -\frac{v_{*e}}{\tau} \left[\eta_i + \frac{\Gamma - 1}{\tau} (1 + \eta_i + \tau) \nabla_{\perp}^2 \right] \frac{\partial \phi}{\partial y} \\ &+ \frac{(\Gamma - 1) \epsilon_n g_i v_{*e}}{\tau} \frac{\partial}{\partial y} \left[\frac{1}{\tau} (1 - f_t + (g_e/g_i) \tau) \phi_k + (1 + \frac{\Gamma}{\Gamma - 1}) T_i + \frac{n}{\tau} \right] \\ &+ \frac{(\Gamma - 1) \epsilon_n g_i v_{*e}}{\tau^2} \nabla_{\perp}^2 \frac{\partial}{\partial y} \left[(1 + \tau) \phi + \frac{\tau}{1 - f_t} T_i + \frac{1 + \tau}{1 - f_t} n + \frac{f_t \tau}{1 - f_t} T_{et} \right] \end{aligned} \quad (4)$$

Equation (1) represents the conservation of effective electron density, Eq. (2) is the electron heat balance, Eq. (3) is charge balance, and Eq. (4) is the ion heat balance. Here, $n = n_{et} + f_t \tilde{\phi}$ is an effective density, with $n_{et} = \int d^3v h_e/n_0$ the trapped electron density [15, 16]. Note that this convention for trapped electrons is a different convention than the one used in the Chalmers model. The quantity ϕ denotes the electric potential, $\tilde{\phi} = \phi - \langle \phi \rangle$, with $\langle \cdot \rangle = \frac{1}{L_y} \int dy$ the flux surface average, and $\mathbf{v}_E = \hat{z} \times \nabla \phi$ denotes the $E \times B$ drift. The electric potential is normalized as $\frac{e\phi}{T_{e0}} \rightarrow \phi$, with T_{e0} a reference electron temperature. The quantity $\nabla_{\perp}^2 = \frac{\partial^2}{\partial x^2} + \frac{\partial^2}{\partial y^2}$ is the perpendicular Laplacian, and x, y, z denote the local radial, poloidal and toroidal directions in a fusion device. Time is normalized as $(c_s/L_n)t \rightarrow t$, with $c_s = \sqrt{T_e}/m_i$ the sound speed, and space is normalized by the gyroradius at the electron temperature $\rho_s = c_s/\omega_{c,i}$, with $\omega_{c,i} = eB/m_i$ the ion gyrofrequency. The quantity $\tau = T_{e0}/T_{i0}$ is the temperature ratio, and $\Gamma = 5/3$ is the adiabatic index. The parameter $f_t = \sqrt{\epsilon}$ is the trapped-electron fraction, with $\epsilon = a/R$ the inverse aspect ratio, and terms proportional to $\epsilon_n = 2L_n/R$ denote magnetic drift effects modeling magnetic drift for ions and toroidal precession-drift for trapped-electrons. The parameter $g_e(s) = \frac{1}{4} + \frac{2}{3}s$ represents the effect of magnetic shear on the precession frequency of trapped-electrons, and $g_i(s) = \frac{2}{3} + \frac{5}{9}s - \epsilon$ is its effect on the magnetic drift for ions [17, 18].

Since we are interested in frequencies $\omega \gg k_{\parallel}c_s$, where c_s is the sound speed, we neglect parallel ion motion.

2.1 Schrödinger-like equation

In this section, we neglect magnetic shear effects, i.e. we assume $g_i = g_e = 1$, for simplicity. Based on Ref. [19], the linearization of the system (1 - 4) can be written in the form of the following 4-component Schrödinger-like equation:

$$i\frac{\partial}{\partial t} \begin{bmatrix} 1 & 0 & 0 & 0 \\ 0 & 1 & 0 & 0 \\ 0 & 0 & 1 - f_t + k_{\perp}^2 & 0 \\ 0 & 0 & 0 & 1 \end{bmatrix} \begin{bmatrix} n_k \\ T_{ek} \\ \phi_k \\ T_{ik} \end{bmatrix} = H \begin{bmatrix} n_k \\ T_{ek} \\ \phi_k \\ T_{ik} \end{bmatrix}, \quad (5)$$

where H denotes the Hamiltonian matrix, given by:

$$H = \begin{bmatrix} a & a & b & 0 \\ c & d & f & 0 \\ g & -a & h & -a \\ j & k & l & m \end{bmatrix}, \quad (6)$$

where $a - m$ are real-valued coefficients given by:

$$a = \omega_{de}, \quad b = f_t(\omega_* - \omega_{de}), \quad (7)$$

$$c = \frac{2}{3}\omega_{de}, \quad d = \frac{7}{3}\omega_{de}, \quad f = f_t(\eta_e\omega_* - \frac{2}{3}\omega_{de}), \quad (8)$$

$$g = -(1 + \frac{1}{\tau})\omega_{de}, \quad h = (1 - f_t - \frac{1 + \eta_i}{\tau}k_{\perp}^2)\omega_* - (1 - f_t)(1 + \frac{1}{\tau})\omega_{de}, \quad (9)$$

$$j = -\frac{2}{3\tau^2}(1 - \frac{1 + \tau}{1 - f_t}k_{\perp}^2)\omega_{de}, \quad k = \frac{2}{3\tau} \frac{k_{\perp}^2}{1 - f_t}\omega_{de}, \quad (10)$$

$$l = \frac{1}{\tau} \left[(\eta_i - \frac{2}{3\tau}(1 + \eta_i + \tau)k_{\perp}^2)\omega_* - \frac{2}{3\tau}(1 - f_t + \tau - (1 + \tau)k_{\perp}^2)\omega_{de} \right], \quad (11)$$

$$m = -(\frac{7}{3} - \frac{2}{3} \frac{k_{\perp}^2}{1 - f_t}) \frac{\omega_{de}}{\tau} \quad (12)$$

To obtain the ‘normal coordinates’, i.e. the eigenvectors associated to this system, one needs to diagonalize the H matrix.

Later on, we will focus on the ‘pure’ CTEM turbulence, i.e. ∇T_e -driven CTEM. That is, considering quasi-neutrality $n_i = n + (1 - f_t)[\phi - \langle \phi \rangle]$, we assume that the mode frequency resonates with the precession-drift frequency,

i.e. $\omega_k \sim \frac{5}{3}\omega_{de}$. Hence, we use the approximation:

$$|n_i| \ll |n|, |\phi - \langle \phi \rangle| \quad (13)$$

In this regime, the electron dynamics decouples from the ion dynamics, and the quasi-neutrality condition reduces to [6] :

$$n \simeq -(1 - f_t)[\phi - \langle \phi \rangle] \quad (14)$$

Hence, in this regime, the effective density fluctuations are proportional to the electric potential fluctuations, and there is no turbulent particle transport. Using approximation (14), the system (1-4) reduces to the following pure CTEM model:

$$\frac{\partial \tilde{\phi}}{\partial t} + \mathbf{v}_E \cdot \nabla \tilde{\phi} - \xi v_{*e} \frac{\partial \phi}{\partial y} = -\epsilon_n v_{*e} \frac{\partial}{\partial y} [(1 + \xi)\phi - \xi T_{et}] \quad (15)$$

$$\frac{\partial T_{et}}{\partial t} + \mathbf{v}_E \cdot \nabla T_{et} + \eta_e v_{*e} \frac{\partial \phi}{\partial y} = \frac{2}{3\xi} \epsilon_n v_{*e} \frac{\partial}{\partial y} [(1 + \xi)\phi - \frac{7}{2}\xi T_{et}], \quad (16)$$

with $\tilde{\phi} = \phi - \langle \phi \rangle$ and $\xi = f_t/(1 - f_t)$.

For now, let us carry on the analysis of the full system (1-4).

2.2 Linear analysis

Linearizing the system (1-4), one obtains:

$$\omega n_k = a(n_k + T_{ek}) + b\phi_k, \quad (17)$$

$$\omega T_{ek} = cn_k + dT_{ek} + f\phi_k, \quad (18)$$

$$(1 - f_t + k_{\perp}^2)\omega\phi_k = gn_k + h\phi_k - a(T_{ek} + T_{ik}), \quad (19)$$

$$\omega T_{ik} = jn_k + kT_{ek} + l\phi_k + mT_{ik}, \quad (20)$$

where the coefficients $a - m$ are given by expressions (7 – 12).

After some algebra, one obtains the following ITG-TEM linear dispersion relation:

$$\frac{(\omega_* + \tau\omega_{di})(\omega - \frac{5}{3}\omega_{di}) - k_{\perp}^2(\omega + \frac{1+\eta_i}{\tau}\omega_*)(\omega - \frac{5}{3}\omega_{di}) + (\eta_i - \frac{7}{3} + \frac{5}{3}\epsilon_n)\omega_*\omega_{di}}{N_i} = \\ f_t \frac{(\omega_* - \omega_{de})(\omega - \frac{5}{3}\omega_{de}) + (\eta_e - \frac{2}{3})\omega_*\omega_{de}}{N_e} + 1 - f_t, \quad (21)$$

where the denominators are $N_i = \omega^2 - \frac{10}{3}\omega_{di}\omega + \frac{5}{3}\omega_{di}^2$ and $N_e = \omega^2 - \frac{10}{3}\omega_{de}\omega + \frac{5}{3}\omega_{de}^2$. Details of the derivation are given in Appendix. Eq. (21) is a quartic dispersion relation which describes two coupled modes, an electron mode (CTEM rotating in the electron diamagnetic direction), and an ion mode (ITG rotating in the ion diamagnetic direction) [6]. As we focus here on trapped electron mode turbulence, we assume $\eta_i \ll \eta_e$, and thus the electron branch (CTEM branch) is dominant. It resonates close to the toroidal precession drift frequency $\omega_k \propto \omega_{de}$. In the ∇T_e -driven CTEM regime, $|N_i| \gg |N_e|$. Hence the dispersion relation reduces to a quadratic, and the CTEM mode resonates at the frequency $\omega_k = \omega_{\text{res}} = \frac{5}{3}\omega_{de}$. We are talking here about a fluid resonance, which is an approximation of the kinetic resonance [2].

From the linearized Eqs. (17, 18, 19, 20), one obtains - after some algebra - the following system:

$$[\omega - \omega_{de} + \Lambda_k^{\text{TEM}}]n_k - f_t\omega_{de}(s_{ek} + \frac{2}{3f_t}n_k) - \Lambda_k^{\text{TEM}}n_{ik} = 0, \quad (22)$$

$$\omega s_{ek} - \frac{5}{3}\omega_{de}(s_{ek} + \frac{2}{3f_t}n_k) + (\eta_e - \frac{2}{3})\frac{\omega_*}{1-f_t}n_k - (\eta_e - \frac{2}{3})\frac{\omega_*}{1-f_t}n_{ik} = 0, \quad (23)$$

$$\omega s_{ik} - \frac{5}{3}\omega_{di}(s_{ik} + \frac{2}{3\tau}n_{ik}) + (\eta_i - \frac{2}{3})\frac{\omega_*/\tau}{1-f_t}n_k - (\eta_i - \frac{2}{3})\frac{\omega_*/\tau}{1-f_t}n_{ik} = 0, \quad (24)$$

$$\Lambda_k^{\text{ITG}}n_k + [\omega - \omega_{di} - \Lambda_k^{\text{ITG}}]n_{ik} - \tau\omega_{di}(s_{ik} + \frac{2}{3\tau}n_{ik}) = 0, \quad (25)$$

where we used quasi-neutrality to express the electric potential: $\phi_k = \frac{1}{1-f_t}(n_{ik} - n_k)$, the parameters $\Lambda_k^{\text{TEM}} = \xi(\omega_* - \omega_{de})$ and $\Lambda_k^{\text{ITG}}(\omega) = \frac{1}{1-f_t} \left[(1 - \frac{1+\eta_i}{\tau}k_\perp^2) \omega_* + \tau\omega_{di} - k_\perp^2\omega \right]$ were defined, and $\xi = f_t/(1-f_t)$. The following quantities were introduced:

$$s_{ik} = T_{ik} - \frac{2}{3\tau}n_{ik}, \quad \text{and} \quad s_{ek} = T_{ek} - \frac{2}{3f_t}n_k, \quad (26)$$

where s_{ik} (s_{ek}) is the thermodynamic entropy for ions (electrons), as described for ITG in Refs. [20, 21].

In matrix form, the ITG-TEM system takes the simple form:

$$\begin{bmatrix} \omega - \frac{5}{3}\omega_{de} + \Lambda_k^{\text{TEM}} & -f_t\omega_{de} & -\Lambda_k^{\text{TEM}} & 0 \\ (\eta_e - \frac{2}{3})\frac{\omega_*}{1-f_t} - \frac{10}{9f_t}\omega_{de} & \omega - \frac{5}{3}\omega_{de} & -(\eta_e - \frac{2}{3})\frac{\omega_*}{1-f_t} & 0 \\ \Lambda_k^{\text{ITG}}(\omega) & 0 & \omega - \frac{5}{3}\omega_{di} - \Lambda_k^{\text{ITG}}(\omega) & -\tau\omega_{di} \\ (\eta_i - \frac{2}{3})\frac{\omega_*/\tau}{1-f_t} & 0 & -\left[(\eta_i - \frac{2}{3})\frac{\omega_*/\tau}{1-f_t} + \frac{10}{9\tau}\omega_{di}\right] & \omega - \frac{5}{3}\omega_{di} \end{bmatrix} \begin{bmatrix} n_k \\ s_{ek} \\ n_{ik} \\ s_{ik} \end{bmatrix} = 0 \quad (27)$$

This form of the ITG-TEM system clearly shows that the system is almost block-diagonal, with the coupling between the two branches occurring only through the effective electron density n_k and the ion density n_{ik} . The two branches decouple in the following two limits: i) The toroidal ITG mode is recovered in the limit of negligible trapped electron fraction $f_t \rightarrow 0$ corresponding to Boltzmann electrons, for which the effective electron density is negligible $|n_k| \ll |n_{ik}|, |s_{ik}|$. It corresponds to the lower block-diagonal. Note that the total electron density in this case is simply $n_{ek} = n_{ik} \simeq \phi_k$. ii) The pure-CTEM mode, i.e. ∇T_e -driven CTEM is recovered in the limit $|n_{ik}| \ll |n_k|, |s_{ek}|$. It corresponds to the upper block-diagonal.

An alternative way to represent the system is in terms of the ion gyro-center density $n_i^{\text{GC}} = n_i - \nabla_{\perp}^2 \phi$ instead of ion density n_i . Then, the electric potential is given by $\phi_k = \frac{1}{1-f_t+k_{\perp}^2}(n_{ik}^{\text{GC}} - n_k)$, and the system can be written in the form of the following Schrödinger-like equation:

$$i \frac{\partial}{\partial t} \Psi = \begin{bmatrix} \frac{5}{3}\omega_{de} - \Lambda_k^{\text{TEM}} & f_t\omega_{de} & \Lambda_k^{\text{TEM}} & 0 \\ -\left[(\eta_e - \frac{2}{3})\frac{\omega_*}{1-f_t+k_{\perp}^2} - \frac{10}{9f_t}\omega_{de}\right] & \frac{5}{3}\omega_{de} & (\eta_e - \frac{2}{3})\frac{\omega_*}{1-f_t+k_{\perp}^2} & 0 \\ -\Lambda_k^{\text{GC}} & 0 & \frac{5}{3}\omega_{di} + \Lambda_k^{\text{GC}} & \tau\omega_{di} \\ -(\eta_i - \frac{2}{3})\frac{\omega_*/\tau}{1-f_t+k_{\perp}^2} & 0 & (\eta_i - \frac{2}{3})\frac{\omega_*/\tau}{1-f_t+k_{\perp}^2} + \frac{10}{9\tau}\omega_{di} & \frac{5}{3}\omega_{di} \end{bmatrix} \Psi, \quad (28)$$

where $\Psi = [n_k, s_{ek}, n_{ik}^{\text{GC}}, s_{ik}]^T$ is the eigenvector, the coefficient $\Lambda_k^{\text{ITG}}(\omega)$ is now replaced by $\Lambda_k^{\text{GC}} = \frac{1}{1-f_t+k_{\perp}^2} \left[(1 - \frac{1+\eta_i}{\tau} k_{\perp}^2) \omega_* + \tau\omega_{di} - \frac{5}{3} k_{\perp}^2 \omega_{di} \right]$ which does not depend on the complex frequency ω , and Λ_k^{TEM} is now defined as $\Lambda_k^{\text{TEM}} = \xi_k(\omega_* - \omega_{de})$, where the trapping parameter $\xi_k = f_t/(1 - f_t + k_{\perp}^2)$ now depends on the squared wavenumber k_{\perp}^2 .

2.3 Crossphase dynamics

To analyze the crossphase dynamics, it is convenient to re-write Eqs. (22), (23) and (24) in terms of n_k , s_{ek} , s_{ik} and the electric potential ϕ_k :

$$\left[\omega - \frac{5}{3}\omega_{de} \right] n_k - f_t\omega_{de}s_{ek} - f_t(\omega_* - \omega_{de})\phi_k = 0 \quad (29)$$

$$(\omega - \frac{5}{3}\omega_{de})s_{ek} - (\eta_e - \frac{2}{3})\omega_*\phi_k - \frac{10}{9f_t}\omega_{de}n_k = 0 \quad (30)$$

$$(\omega - \frac{5}{3}\omega_{di})s_{ik} - \left[(\eta_i - \frac{2}{3})\omega_* + (1 - f_t)\frac{10}{9\tau}\omega_{di} \right] \phi_k - \frac{10}{9\tau}\omega_{di}n_k = 0 \quad (31)$$

Let us define the 3 crossphases:

$$\theta_k = \arg\left(\frac{\phi_k}{n_k}\right), \quad \zeta_k = \arg\left(\frac{\phi_k}{s_{ek}}\right), \quad \chi_k = \arg\left(\frac{\phi_k}{s_{ik}}\right) \quad (32)$$

With these definitions, the turbulent particle flux is $\Gamma = \sum_k k_y |n_k| |\phi_k| \sin \theta_k$, and the electron/ion entropy fluxes are $\sum_k k_y |s_{ek}| |\phi_k| \sin \zeta_k$ and $\sum_k k_y |s_{ik}| |\phi_k| \sin \chi_k$, respectively. The ion and electron entropy fluxes are related to the ion and electron heat fluxes $Q_{e,i}$ via $\sum_k k_y \text{Im } \phi_k^* s_{ek} = Q_e - \frac{2}{3f_t} \Gamma$, and $\sum_k k_y \text{Im } \phi_k^* s_{ik} = Q_i - \frac{2}{3\tau} \Gamma$, where use has been made of the quasi-neutrality condition $n_{ik} = n_k + (1 - f_t) \phi_k$.

We use the following ansatz:

$$\begin{bmatrix} \phi_k \\ n_k \\ s_{ek} \\ s_{ik} \end{bmatrix} = \begin{bmatrix} |\phi_k| \\ |n_k| e^{-i\theta_k} \\ |s_{ek}| e^{-i\zeta_k} \\ |s_{ik}| e^{-i\chi_k} \end{bmatrix} e^{-i\omega_k t}, \quad (33)$$

where ω_k is the linear mode frequency.

Replacing n_{ik} , n_k , s_{ek} and s_{ik} in Eqs. (29-31), using the ansatz (33), one obtains, after some algebra, the following system:

$$\begin{aligned} \gamma_k e^{-i\theta_k} |n_k| - i |n_k| e^{-i\theta_k} \left[\frac{\partial \theta_k}{\partial t} + \omega_k \right] &= -\frac{5}{3} i \omega_{de} |n_k| e^{-i\theta_k} \\ &\quad - i f_t \omega_{de} |s_{ek}| e^{-i\zeta_k} - i f_t (\omega_* - \omega_{de}) |\phi_k|, \end{aligned} \quad (34)$$

$$\begin{aligned} \gamma_k e^{-i\zeta_k} |s_{ek}| - i |s_{ek}| e^{-i\zeta_k} \left[\frac{\partial \zeta_k}{\partial t} + \omega_k \right] &= -\frac{5}{3} i \omega_{de} |s_{ek}| e^{-i\zeta_k} \\ &\quad - i (\eta_e - \frac{2}{3}) \omega_* |\phi_k| - i \frac{10}{9f_t} \omega_{de} |n_k| e^{-i\theta_k}, \end{aligned} \quad (35)$$

$$\begin{aligned} \gamma_k e^{-i\chi_k} |s_{ik}| - i |s_{ik}| e^{-i\chi_k} \left[\frac{\partial \chi_k}{\partial t} + \omega_k \right] &= -\frac{5}{3} i \omega_{di} |s_{ik}| e^{-i\chi_k} \\ &\quad - i \left[(\eta_i - \frac{2}{3\tau}) \omega_* + (1 - f_t) \frac{10}{9\tau} \omega_{di} \right] |\phi_k| - i \frac{10}{9\tau} \omega_{di} |n_k| e^{-i\theta_k}, \end{aligned} \quad (36)$$

where we used $\partial_t |u_k| = \gamma_k |u_k|$, for $u_k = n_k, s_{ek}, s_{ik}$. It is apparent that Eqs. (34,35) can be solved independently from Eq. (36). Physically, the crossphase χ_k responsible for ion thermal transport does not influence the crossphases θ_k and ζ_k associated to electron transport. We will thus first solve for the electron crossphases. One can separate the real and imaginary parts of Eqs.

(34,35). The real part yields two relations between the crossphases θ_k , ζ_k and the linear growth-rate:

$$\gamma_k = f_t(\omega_* - \omega_{de})\alpha_k \sin \theta_k + f_t \omega_{de} \frac{\alpha_k}{\beta_k} \sin \psi_k, \quad (37)$$

$$\gamma_k = -\frac{10}{9f_t} \omega_{de} \frac{\beta_k}{\alpha_k} \sin \psi_k + (\eta_e - \frac{2}{3}) \omega_* \beta_k \sin \zeta_k, \quad (38)$$

where $\gamma_k = |n_k|^{-1} \partial_t |n_k| = |s_{ek}|^{-1} \partial_t |s_{ek}| = |s_{ik}|^{-1} \partial_t |s_{ik}|$ is the linear growth-rate, and $\psi_k = \theta_k - \zeta_k$ is the crossphase mismatch responsible for transport decoupling between particle transport v.s. electron heat transport. The quantities α_k and β_k are the two amplitude ratios defined as:

$$\alpha_k = \frac{|\phi_k|}{|n_k|}, \quad \beta_k = \frac{|\phi_k|}{|s_{ek}|}, \quad (39)$$

and $\alpha_k/\beta_k = |s_{ek}|/|n_k|$ is the third amplitude ratio.

The imaginary part of Eqs. (34,35) yields the following crossphase dynamics.

$$\frac{\partial \theta_k}{\partial t} = \omega_{\text{res}} - \omega_k + f_t(\omega_* - \omega_{de})\alpha_k \cos \theta_k + f_t \omega_{de} \frac{\alpha_k}{\beta_k} \cos \psi_k, \quad (40)$$

$$\frac{\partial \zeta_k}{\partial t} = \omega_{\text{res}} - \omega_k + \frac{10}{9f_t} \omega_{de} \frac{\beta_k}{\alpha_k} \cos \psi_k + (\eta_e - \frac{2}{3}) \omega_* \beta_k \cos \zeta_k, \quad (41)$$

$$\frac{\partial \psi_k}{\partial t} = \left(f_t \frac{\alpha_k}{\beta_k} - \frac{10}{9f_t} \frac{\beta_k}{\alpha_k} \right) \omega_{de} \cos \psi_k + f_t(\omega_* - \omega_{de})\alpha_k \cos \theta_k - (\eta_e - \frac{2}{3}) \omega_* \beta_k \cos \zeta_k, \quad (42)$$

where $\omega_{\text{res}} = \frac{5}{3}\omega_{de}$ is the resonance frequency. Here, Eq. (42) is the difference of Eq. (40) and Eq. (41). Considering the amplitude ratio system (37,38), it is convenient to define the inverse amplitude ratios $A_k = 1/\alpha_k$ and $B_k = 1/\beta_k$. After some algebra, one obtains the following matrix system:

$$\begin{bmatrix} \gamma_k & f_t \omega_{de} \sin \psi_k \\ -\frac{10}{9f_t} \omega_{de} \sin \psi_k & \gamma_k \end{bmatrix} \begin{bmatrix} A_k \\ B_k \end{bmatrix} = \begin{bmatrix} f_t(\omega_* - \omega_{de}) \sin \theta_k \\ (\eta_e - \frac{2}{3}) \omega_* \sin \zeta_k \end{bmatrix} \quad (43)$$

Inverting the matrix yields after some algebra:

$$\frac{1}{\alpha_k} = \frac{f_t[(1 - \epsilon_n)\omega_*/\gamma_k] \sin \theta_k - f_t(\eta_e - \frac{2}{3})(\epsilon_n \omega_*^2/\gamma_k^2) \sin \zeta_k \sin \psi_k}{1 + \frac{10}{9} \epsilon_n^2 (\omega_*^2/\gamma_k^2) \sin^2 \psi_k}, \quad (44)$$

$$\frac{1}{\beta_k} = \frac{(\eta_e - \frac{2}{3})(\omega_*/\gamma_k) \sin \zeta_k + \frac{10}{9}[(1 - \epsilon_n)\epsilon_n \omega_*^2/\gamma_k^2] \sin \theta_k \sin \psi_k}{1 + \frac{10}{9} \epsilon_n^2 (\omega_*^2/\gamma_k^2) \sin^2 \psi_k}, \quad (45)$$

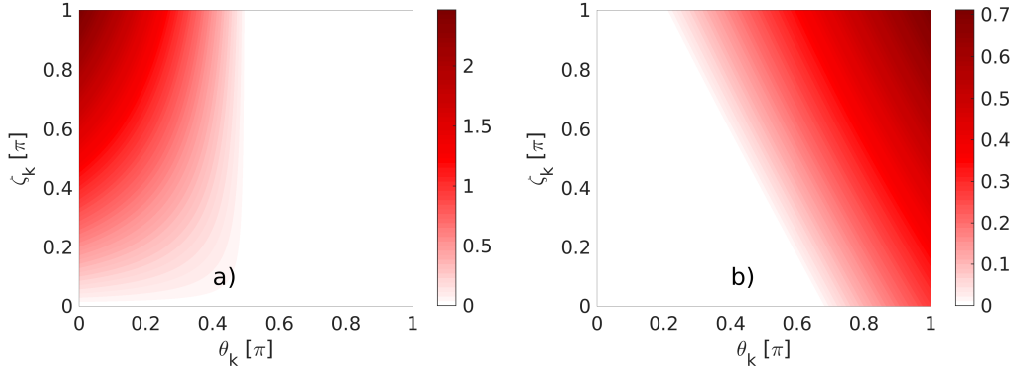


Figure 1: Amplitude ratios for ITG/TEM: a) inverse amplitude ratio $A_k = \frac{1}{\alpha_k}$ and b) $B_k = \frac{1}{\beta_k}$, expressions (44,45) v.s. θ_k and ζ_k , for the parameters $\eta_e = 2$, $\epsilon_n = 0.8$ and $\gamma_k/\omega_* = 1$.

The inverse amplitude ratios A_k and B_k , expressions (44,45) are plotted v.s. θ_k and ζ_k , for the parameters $\eta_e = 2$, $\epsilon_n = 0.8$ and $\gamma_k/\omega_* = 1$ [Fig.1]. Values on the forbidden domains - since A_k and B_k are amplitudes, they must be positive - are set to zero for clarity.

Alternatively, this can also be written:

$$\alpha_k = \frac{\gamma_k/\omega_*}{f_t(1 - \epsilon_n) \sin \theta_k + \frac{1}{\beta_k} f_t \epsilon_n \sin \psi_k} \quad (46)$$

$$\beta_k = \frac{\gamma_k/\omega_*}{(\eta_e - \frac{2}{3}) \sin \zeta_k - \frac{1}{\alpha_k} \cdot \frac{10}{9f_t} \epsilon_n \sin \psi_k} \quad (47)$$

It is clear from Eqs. (46,47) that the two amplitude ratios α_k and β_k are coupled. One identifies two opposite regimes: $\frac{1}{\beta_k} \ll 1$, corresponding to negligible electron heat transport, and $\frac{1}{\alpha_k} \ll 1$ corresponding to negligible particle transport. In the following, we will focus on the latter case, since we assume $\epsilon_n \sim 1$. In the regime $\frac{1}{\alpha_k} \ll 1$, the turbulence corresponds to ∇T_e -driven CTEM. In this regime, one may neglect the coupling of the amplitude ratio β_k to α_k , i.e. one uses the approximation:

$$\beta_k \simeq \frac{\gamma_k}{(\eta_e - \frac{2}{3}) \omega_* \sin \zeta_k} \quad (48)$$

Then, the dynamics of the crossphase ζ_k decouples from the other crossphases

θ_k and ψ_k , and reduces to:

$$\frac{\partial \zeta_k}{\partial t} \simeq -(\omega_k - \omega_{\text{res}}) + \gamma_k \cot \zeta_k, \quad (49)$$

where $\cot \zeta_k = 1/\tan \zeta_k$ is the cotangent of the crossphase.

2.4 ITG limit

Linearizing the original ITG-TEM system (1-4), one obtains:

$$-i\omega n_k + if_t \omega_* \phi_k = -i\epsilon_n g_e \omega_* (n_k - f_t \phi_k + f_t T_{ek}), \quad (50)$$

$$-i\omega T_{ek} + i\eta_e \omega_* \phi_k = -\frac{2}{3f_t} i\epsilon_n g_e \omega_* (n_k - f_t \phi_k + \frac{7}{2} f_t T_{ek}), \quad (51)$$

$$-(1 - f_t + k_\perp^2) i\omega \phi_k + i(1 - f_t - \frac{1 + \eta_i}{\tau} k_\perp^2) \omega_* \phi_k = i\epsilon_n g_e \omega_* [(1 - f_t)(1 + g_i/(g_e \tau)) \phi_k + (g_i/g_e) T_{ik} + (1 + g_i/(g_e \tau)) n_k + f_t T_{ek}], \quad (52)$$

$$\begin{aligned} -i\omega T_{ik} = i \frac{\epsilon_n g_e \omega_*}{\tau} & \left[\frac{2}{3\tau} (1 - f_t + \tau) \phi_k + \frac{2}{3\tau} n_k + \frac{7}{3} T_{ik} \right] - i \left[\eta_i - \frac{2}{3\tau} (1 + \eta_i + \tau) k_\perp^2 \right] \frac{\omega_*}{\tau} \phi_k \\ & - \frac{2}{3\tau^2} i k_\perp^2 \epsilon_n g_e \omega_* \left[(1 + \tau) \phi_k + \frac{\tau}{1 - f_t} T_{ik} + \frac{1 + \tau}{1 - f_t} n_k + \frac{\tau f_t}{1 - f_t} T_{ek} \right], \end{aligned} \quad (53)$$

with $\omega_* = k_y v_{*e}$ the electron diamagnetic frequency. The linear dispersion relation is best obtained by first transforming the system. Adding Eqs. (50) and (52) yields the ion continuity equation:

$$-i\omega (n_{ik} + k_\perp^2 \phi_k) + \left(1 - \frac{1 + \eta_i}{\tau} k_\perp^2\right) i\omega_* \phi_k = i \frac{\epsilon_n g_i \omega_*}{\tau} \left[(1 - f_t + \tau) \phi_k + n_k + \tau T_{ik} \right], \quad (54)$$

where $n_{ik} = n_k + (1 - f_t) \phi_k$ is the ion density perturbation set by quasi-neutrality (this is the particle - not gyrocenter - density). In the ITG limit, i.e. without trapped-electrons $f_t \rightarrow 0$, the ion continuity equation and ion heat balance become:

$$-i\omega (n_{ik} + k_\perp^2 \phi_k) + \left(1 - \frac{1 + \eta_i}{\tau} k_\perp^2\right) i\omega_* \phi_k = i \frac{\epsilon_n g_i \omega_*}{\tau} \left[(1 + \tau) \phi_k + n_{ik} + \tau T_{ik} \right], \quad (55)$$

$$(-i\omega - i \frac{5 \epsilon_n g_i \omega_*}{3\tau}) T_{ik} + \frac{2}{3\tau} i\omega n_{ik} = \frac{2}{3\tau} (\eta_i - \frac{2}{3}) i\omega_* \phi_k \quad (56)$$

Defining $\tau_i = T_i/T_e = 1/\tau$, the ion continuity Eq. (54) and ion heat

balance Eq. (20) become, respectively:

$$-i\omega n_{ik} + (-i\omega - i\alpha_i k_y) k_\perp^2 \phi_k + i k_y \phi_k - i \tau_i \epsilon_n g_i k_y [(1 + \frac{1}{\tau_i}) \phi_k + n_{ik} + \frac{T_{ik}}{\tau_i}] = 0, \quad (57)$$

$$-i\omega T_{ik} - i k_y \frac{5}{3} \tau_i \epsilon_n g_i T_{ik} + (\eta_i - \frac{2}{3}) i \tau_i k_y \phi_k + \frac{2}{3} i \tau_i \omega n_{ik} = 0, \quad (58)$$

with $\alpha_i = \tau_i(1 + \eta_i)$. Here, the fields have been further normalized as $n_{ik} \rightarrow \frac{L_n}{\rho_s} n_{ik}$, and same for T_{ik} . For ITG, electrons are Boltzmann $n_{ik} = \phi_k$. From Eq. (58), one obtains after some algebra the following linear response of ion temperature to potential :

$$T_{ik} = \frac{(\eta_i - \frac{2}{3}) \tau_i k_y + \frac{2}{3} \tau_i \omega}{\omega + \frac{5}{3} \tau_i \epsilon_n g_i k_y} \phi_k \quad (59)$$

Replacing T_{ik} in Eq. (57) using the response (59), one obtains - after some algebra - the following quadratic dispersion relation:

$$A\omega^2 + B\omega + C = 0, \quad (60)$$

with real-valued coefficients given by $A = 1 + k_\perp^2$, $B = 2k_y \left[\frac{5}{3} \tau_i \epsilon_n g_i - \frac{1}{2} (1 - \epsilon_n g_i) + \frac{k_\perp^2}{2} (\alpha_i + \frac{5}{3} \tau_i \epsilon_n g_i) \right]$ and $C = \tau_i \epsilon_n g_i k_y^2 \left[\eta_i - \frac{7}{3} + \frac{5}{3} (1 + \tau_i) \epsilon_n g_i + \frac{5}{3} \alpha_i k_\perp^2 \right]$. The solution to the ITG dispersion relation (60) is then:

$$\omega_{1,2} \simeq -\frac{B}{2A} \pm \frac{1}{2A} \sqrt{B^2 - 4AC} \quad (61)$$

The unstable branch has a growth-rate $\gamma_k \simeq \frac{1}{\sqrt{A}} \sqrt{C - \frac{B^2}{4A}} = \frac{1}{\sqrt{A}} \sqrt{C - A(\frac{B}{2A})^2}$. After some algebra, the ITG frequency and growth-rate are given by:

$$\omega_k^{\text{ITG}} \simeq \frac{-k_y}{1 + k_\perp^2} \left[\frac{5}{3} \tau_i \epsilon_n g_i - \frac{1}{2} (1 - \epsilon_n g_i) + \frac{k_\perp^2}{2} (\alpha_i + \frac{5}{3} \tau_i \epsilon_n g_i) \right], \quad (62)$$

$$\gamma_k^{\text{ITG}} \simeq \frac{k_y \sqrt{\tau_i \epsilon_n g_i}}{\sqrt{1 + k_\perp^2}} \sqrt{\eta_i - \eta_i^c}, \quad (63)$$

where $\eta_i^c = \frac{1}{\tau_i \epsilon_n g_i} (1 + k_\perp^2) \frac{\omega_k^2}{k_y^2} + \frac{7}{3} - \frac{5}{3} (1 + \tau_i) \epsilon_n g_i - \frac{5}{3} \alpha_i k_\perp^2$ is the linear ITG threshold, with $\omega_k = \omega_k^{\text{ITG}}$ [22]. Note that here the growth-rate has a factor $\sqrt{1 + k_\perp^2}$ in the denominator, compared to the factor $(1 + k_\perp^2)$ in Ref. [22].

We believe there was a typo in [22].

The analytic expressions for the real ITG frequency (62) and growth-rate (63) are compared to Eqs. (13b,13c) in Nilsson *et al.* [4], and to linear gyrokinetic simulations with the global gyrokinetic code GKPSP which includes fully gyrokinetic ions and bounce-averaged kinetic electrons [11]. Here, Boltzmann electrons are used for the comparison. To take into account magnetic shear effects, the perpendicular wavenumber k_\perp^2 is replaced by its average over a ballooning trial function, yielding $\langle k_\perp^2 \rangle = [1 + (\pi^2 - 7.5)s^2/3]k_y^2$ [23]. The parameters are $R/L_n = 2$, $R/L_{Ti} = 6$, $R/L_{Te} \simeq 0$, and $T_i/T_e = 1$. The safety factor is $q = 1.34$ and the magnetic shear $s = 0.75$. The ITG frequency given by expression (62) is plotted v.s. k_y (squares) and compared to the GKPSP result (diamonds) and to the analytical expression (13b) of Nilsson *et al.* [4] [Fig.2a]. The frequency of the ITG fluid model only shows qualitative similarity with the GKPSP data, but our analytical result shows better agreement with GKPSP data than Ref. [4], especially at large $k_y\rho_s$. This is probably due to the different treatment of ion FLR effects.

The ITG growth-rate given by expression (63) is plotted v.s. k_y (squares) and compared to the Nilsson expression (13c) in Ref. [4] (black), and to the GKPSP result (diamonds) [Fig.2b]. The growth-rate also shows qualitative similarity, although the growth-rate of the fluid model is much larger than the GKPSP result and peaks at a slightly higher wavenumber. The result from Ref. [4] seems to show closer agreement with the GKPSP data at small $k_y\rho_s$. However, the growth-rate peaks at $k_y\rho_s > 1$, which is unphysical. This shows that the formula of Ref. [4] is only valid for $k_y\rho_s \ll 1$.

We also plot the ITG growth-rate - normalized to ω_* - v.s. the parameter ϵ_n [Fig.3], in the case $\eta_i = 2$, $k_\perp^2 = 0$ and $\tau_i = 1$. Previous analytical results are also plotted, for comparison. In particular, in the Introduction section of Beer's PhD thesis [24], the ITG growth-rate from a 'simple fluid' model is compared to results from the '3+1 Gyro-Landau-Fluid' model. We cannot compare our results to the latter, as we don't have access to this data, but a comparison is made with the 'simple fluid' case. Note that here, $\epsilon_n = 2L_n/R$ as opposed to L_n/R in Ref. [24]. At the value $\epsilon_n \sim 1$ - relevant for core plasmas - one can see that expression (63) gives a lower growth-rate than the simple fluid model in Ref. [24], and the Jarmen *et al.* [5] formula, which are more consistent with the 'gyrofluid' and 'kinetic' value of $\gamma/\omega_* \simeq 0.4$ at $\epsilon_n = 1$ in Ref. [24] (not shown). The Nilsson formula from Ref. [4] has even better agreement with the latter results, compared to expression (63).

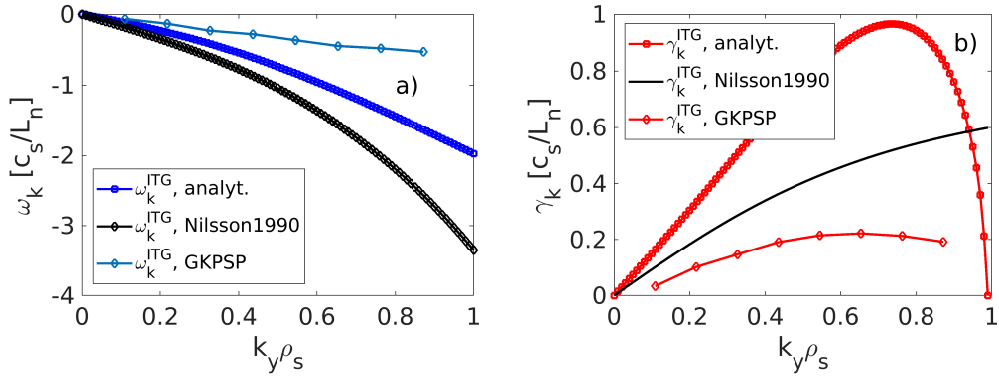


Figure 2: Comparison of the analytical model with Nilsson *et al.* 1990 [4] and with gyrokinetic simulations: a) ITG frequency and b) ITG growth-rate v.s. poloidal wavenumber k_y . The parameters are $\eta_i = 3$, $\epsilon_n = 1$ ($\frac{R}{L_n} = 2$), $T_i/T_e = 1$ and $\eta_e \simeq 0$, with Boltzmann electrons.

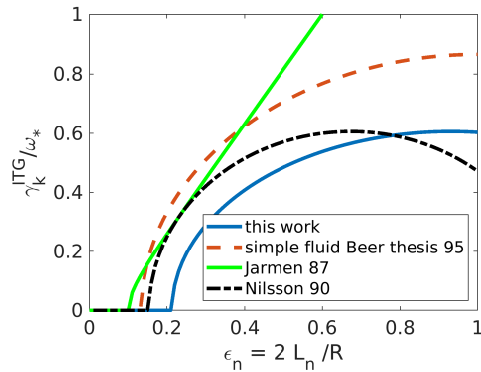


Figure 3: ITG growth-rate v.s. ϵ_n for the analytical model Eq. (63) (blue) and comparison with three previous analytical models: the ‘simple fluid’ model from Beer thesis [24] (red), the result from Jarmen *et al.* 1987 [5] (green), and by Nilsson *et al.* 1990 [4] (black). Other parameters are $\eta_i = 2$, $k_\perp^2 = 0$ and $\tau_i = 1$.

3 ∇T_e -driven CTEM limit

We will now focus on the ‘pure’ CTEM turbulence, i.e. ∇T_e -driven CTEM. That is, considering quasi-neutrality $n_i = n + (1 - f_t)[\phi - \langle \phi \rangle]$, we assume that the mode frequency resonates with the precession-drift frequency, i.e. $\omega_k \sim \frac{5}{3}\omega_{de}$. Hence, we use the approximation:

$$|n_i| \ll |n|, |\phi - \langle \phi \rangle| \quad (64)$$

In this regime, the electron dynamics decouples from the ion dynamics, and the quasi-neutrality condition reduces to [6, 17] :

$$n \simeq -(1 - f_t)[\phi - \langle \phi \rangle] \quad (65)$$

Hence, in this regime, the effective density fluctuations are proportional to the electric potential fluctuations, which implies no turbulent particle transport. This directly implies that the zonal density vanishes $\partial_t \langle n \rangle = 0$. The dynamics of zonal density was analyzed in Refs. [7, 25]. Using approximation (65), the system (1-4) reduces to the following ∇T_e -driven CTEM model:

$$\frac{\partial \tilde{\phi}}{\partial t} + \mathbf{v}_E \cdot \nabla \tilde{\phi} - \xi v_{*e} \frac{\partial \phi}{\partial y} = -\epsilon_n v_{*e} \frac{\partial}{\partial y} [(1 + \xi)\phi - \xi T_{et}] \quad (66)$$

$$\frac{\partial T_{et}}{\partial t} + \mathbf{v}_E \cdot \nabla T_{et} + \eta_e v_{*e} \frac{\partial \phi}{\partial y} = \frac{2}{3\xi} \epsilon_n v_{*e} \frac{\partial}{\partial y} [(1 + \xi)\phi - \frac{7}{2}\xi T_{et}], \quad (67)$$

with $\tilde{\phi} = \phi - \langle \phi \rangle$ and $\xi = f_t/(1 - f_t)$. Note that the connection between the slab geometry of the present model and the standard toroidal action-angle variables is explained in Appendix A of Ref. [21]. The simplified CTEM model (66, 67), which is a limiting case of the original model (1-4) also conserves energy. The ratio ξ is shown v.s. trapped-fraction f_t [Fig.4]. One sees that the parameter ξ is of order unity for $f_t \simeq 0.5$ and increases rapidly for $f_t > 0.5$.

Expressing the potential $\tilde{\phi} \simeq -n/(1 - f_t)$ in terms of effective density n from the quasi-neutrality (65), and applying a Fourier transform $g = g_k(x, t)e^{ik_y y}$, with $g = n, T_{et}$, one obtains, after some algebra:

$$\frac{\partial n_k}{\partial t} - i\xi\omega_* n_k = -i\omega_{de} \left[(1 + \xi)n_k + T_k \right], \quad (68)$$

$$\frac{\partial T_k}{\partial t} - i\xi\eta_e\omega_* n_k = -\frac{2}{3}i\omega_{de} \left[(1 + \xi)n_k + \frac{7}{2}T_k \right], \quad (69)$$

where $T_k = f_t T_{ek}$, and $\omega_{de} = \epsilon_n g_e \omega_*$ is the trapped-electron precession-drift frequency.

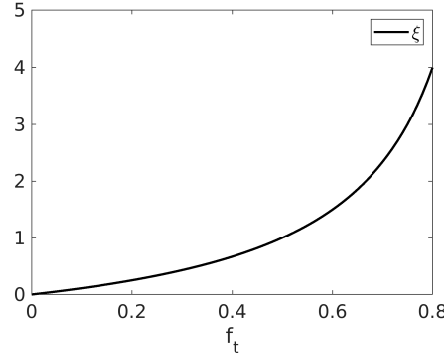


Figure 4: Parameter $\xi = f_t/(1 - f_t)$ v.s. trapped-fraction f_t .

3.1 Schrödinger-like equation for ∇T_e -driven CTEM

The linear CTEM system (68, 69) can be written in the form of a 2-component Schrödinger-like equation:

$$i \frac{\partial}{\partial t} \begin{bmatrix} n_k \\ T_k \end{bmatrix} = \hat{H} \begin{bmatrix} n_k \\ T_k \end{bmatrix}, \quad (70)$$

where the matrix operator \hat{H} denotes the Hamiltonian operator of the system [19]:

$$\hat{H} = \begin{bmatrix} a & b \\ c & d \end{bmatrix}, \quad (71)$$

with coefficients:

$$a = \omega_{de} - \xi(\omega_* - \omega_{de}), \quad b = \omega_{de}, \quad (72)$$

$$c = -\left[\xi\eta_e\omega_* - (1 + \xi)\frac{2}{3}\omega_{de}\right] \leq 0, \quad d = \frac{7}{3}\omega_{de} \quad (73)$$

It is convenient to diagonalize the Hamiltonian matrix. The result is:

$$\begin{bmatrix} \frac{1}{2}(a + d) + i\sqrt{b|c| + ad - \frac{1}{4}(a + d)^2} & 0 \\ 0 & \frac{1}{2}(a + d) - i\sqrt{b|c| + ad - \frac{1}{4}(a + d)^2} \end{bmatrix} \quad (74)$$

This corresponds to a transformation to ‘normal coordinates’:

$$\psi_k^+ = \alpha_k n_k^+ + T_k^+, \quad (75)$$

$$\psi_k^- = \alpha_k^* n_k^- + T_k^-, \quad (76)$$

where the complex-valued parameter α_k is given by:

$$\begin{aligned} \alpha_k &= \frac{d-a}{2|c|} + \frac{i}{|c|} \sqrt{b|c| + ad - \frac{1}{4}(a+d)^2}, \\ &= \frac{\frac{2}{3}\omega_{de} + \frac{\xi}{2}(\omega_* - \omega_{de})}{\xi\eta_e\omega_* - (1+\xi)\frac{2}{3}\omega_{de}} + i \frac{\gamma_k}{\xi\eta_e\omega_* - (1+\xi)\frac{2}{3}\omega_{de}}, \end{aligned} \quad (77)$$

with $\gamma_k = \omega_* \sqrt{\xi\epsilon_n(\eta_e - \eta_e^c)}$ the linear growth-rate and η_e^c the linear threshold given by:

$$\eta_e^c = (1+\xi) \frac{2}{3\xi} \epsilon_n - \frac{7}{3\xi} [\epsilon_n - \xi(1-\epsilon_n)] + \frac{1}{\xi\epsilon_n} \left[\frac{5}{3}\epsilon_n - \frac{\xi}{2}(1-\epsilon_n) \right]^2 \quad (78)$$

Note that the normal coordinates can also be obtained following the method of Ref. [26].

The Schrödinger equation (70) can hence be written in the form:

$$i\frac{\partial}{\partial t} \begin{bmatrix} \psi_k^+ \\ \psi_k^- \end{bmatrix} = H_H \begin{bmatrix} \psi_k^+ \\ \psi_k^- \end{bmatrix} + iH_A \begin{bmatrix} \psi_k^+ \\ \psi_k^- \end{bmatrix}, \quad (79)$$

where $H_H = \frac{1}{2}(\hat{H} + \hat{H}^\dagger)$ and $H_A = \frac{1}{2i}(\hat{H} - \hat{H}^\dagger)$ denote the Hermitian part and anti-Hermitian part of the Hamiltonian. They are given, respectively, as:

$$\begin{aligned} H_H &= \begin{bmatrix} \frac{5}{3}\omega_{de} - \frac{\xi}{2}(\omega_* - \omega_{de}) & 0 \\ 0 & \frac{5}{3}\omega_{de} - \frac{\xi}{2}(\omega_* - \omega_{de}) \end{bmatrix}, \\ H_A &= \gamma_k \sigma_3 = \begin{bmatrix} \gamma_k & 0 \\ 0 & -\gamma_k \end{bmatrix}, \end{aligned} \quad (80)$$

where η_e^c is the linear threshold (78). Here, $\sigma_3 = [(1,0), (0,-1)]$ is one of the three Pauli matrices [27]. The Pauli matrices form a natural base to diagonalize 2×2 systems, so it is a convenient tool for two-field systems[28].

3.2 Linear analysis

After some algebra, one obtains the following quadratic linear dispersion relation:

$$\omega^2 - \left[\frac{10}{3} \omega_{de} - \xi(\omega_* - \omega_{de}) \right] \omega + \omega_{de} \left[\xi \eta_e \omega_* + \frac{7}{3} [\omega_{de} - \xi(\omega_* - \omega_{de})] - (1 + \xi) \frac{2}{3} \omega_{de} \right] = 0 \quad (81)$$

The solution for the linearly unstable branch, with $\omega = \omega_k + i\gamma_k$ is:

$$\omega_k^{\text{CTEM}} = \frac{5}{3} \epsilon_n \omega_* - \frac{\xi}{2} \omega_* (1 - \epsilon_n), \quad (82)$$

$$\begin{aligned} \gamma_k^{\text{CTEM}} &= \sqrt{\xi \eta_e \omega_* \omega_{de} + \frac{7}{3} \omega_{de} [\omega_{de} - \xi(\omega_* - \omega_{de})] - (1 + \xi) \frac{2}{3} \omega_{de}^2 - \omega_k^2} \\ &= \omega_* \sqrt{\xi \epsilon_n (\eta_e - \eta_e^c)}, \end{aligned} \quad (83)$$

where $\omega_k = \omega_k^{\text{CTEM}}$ and η_e^c is the linear CTEM threshold, given by Eq. (78). For the linearly damped branch, the frequency is ω_k^{CTEM} and the linear growth rate is $-\gamma_k^{\text{CTEM}} < 0$. The threshold behaviour - a key feature of CTEM - is recovered in the present simplified model. However, the growth-rate and mode frequency are under-estimated, as shown in the following.

The linear frequency (82) and growth-rate (83) are shown for the parameters $\eta_e = 3.1$, $f_t = 0.5$ and $\epsilon_n = 1$ [Fig. 5], and compared to linear simulations with the global gyrokinetic code GKPSP which includes fully gyrokinetic ions and bounce-averaged kinetic electrons [11]. For the GKPSP simulation, the parameters are $\eta_e = 3.1$, $\epsilon_n = 1$ ($R/L_n = 2$), and $\eta_i = 1$.

The CTEM frequency (blue) and growth-rate (red) are shown v.s. normalized poloidal wavenumber $k_y \rho_s$ for the fluid CTEM model (square) and GKPSP linear simulations (diamonds). The fluid CTEM frequency shows only qualitative similarity with the bounce-averaged kinetic result from GKPSP. Namely, both frequencies increase with increasing wavenumber. For low wavenumber $k_y \rho_s < 0.2$, the fluid ITG frequency seems to approximately match the gyrokinetic result. For the growth-rate also, there is a large discrepancy between the fluid model compared to the GKPSP result, except for $k_y \rho_s < 0.2$. The fluid CTEM model has a growth-rate that increases linearly with $k_y \rho_s$, whereas the growth-rate becomes almost flat at large $k_y \rho_s$ in the GKPSP simulation. The disagreement is not surprising since the fluid ∇T_e -driven CTEM model lacks any inertial/polarization effects ($k_\perp^2 \rho_s^2$).

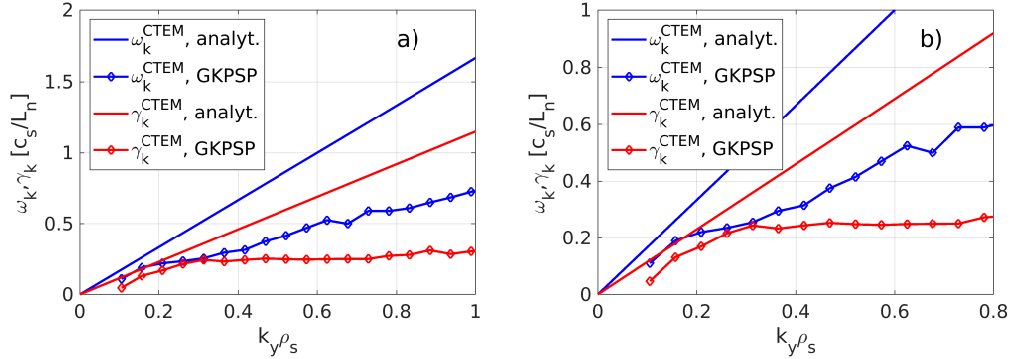


Figure 5: a) Linear growth-rate (red) and frequency (blue) of ∇T_e -driven CTEM two-field model (solid line), and comparison with GKPSP gyrokinetic simulations with bounce-kinetic electrons (diamonds). The parameters are $\eta_e = 3.1$, $f_t = 0.5$ and $\epsilon_n = 1$ ($\frac{R}{L_n} = 2$), and $\eta_i = 1$, and b) close-up for $k_y \rho_s < 0.8$.

3.3 Crossphase dynamics for ∇T_e -driven CTEM

In the ∇T_e -driven CTEM model, there is only a single crossphase ζ_k , the one responsible for electron thermal transport, since particle transport is negligible in this model. The crossphase between electron temperature fluctuations T_{ek} and potential fluctuations ϕ_k is defined as:

$$\zeta_k = \arg\left(\frac{\phi_k}{T_{ek}}\right) = \arg\left(\frac{\phi_k}{s_{ek}}\right) \quad (84)$$

We now apply to the ∇T_e -driven model (70) the same analysis as in section 2.3. It is straightforward to show that the dynamics of the crossphase ζ_k takes the form:

$$\frac{\partial \zeta_k}{\partial t} = \omega_{\text{res}} - \omega_k + \gamma_k \cot \zeta_k, \quad (85)$$

where $\cot \zeta_k = 1 / \tan \zeta_k$ is the cotangent of the crossphase, and $\omega_{\text{res}} = \frac{5}{3} \omega_{de}$ is the resonance frequency. Here, the phase-locked condition $\partial_t \zeta_k = 0$ yields the linear crossphase ζ_k^0 , used in quasi-linear transport analysis. It is given

by:

$$\begin{aligned}\zeta_k^0 &= \arctan\left(\frac{\gamma_k}{\omega_k - \omega_{\text{res}}}\right) \\ &= -\arctan\left(\frac{\sqrt{\xi\epsilon_n(\eta_e - \eta_e^c)}}{\xi(1 - \epsilon_n)}\right) \leq 0,\end{aligned}\quad (86)$$

where \arctan denotes the arctangent function. Hence the crossphase dynamics for ∇T_e -driven CTEM is similar to the Kuramoto equation for coupled phase-oscillators [29]. In the Kuramoto-like Eq. (85), the first term on the r.h.s. $\omega_{\text{res}} - \omega_k$ is the ‘entrainment frequency’ responsible for *phase-mixing*. Recall that $\omega_k = \frac{5}{3}\omega_{de} - \xi\omega_*(1 - \epsilon_n)$ for CTEM. Hence, for CTEM the entrainment frequency takes the form $\omega_{\text{res}} - \omega_k = \xi\omega_*(1 - \epsilon_n) \geq 0$. The last term on the r.h.s. of Eq. (85) is the ‘pinning force’, responsible for *phase-locking*. Like in the Kuramoto model, there exists a threshold above which *synchronization* occurs. This synchronization threshold is here given by:

$$\gamma_k \geq |\omega_k - \omega_{\text{res}}| \quad (87)$$

This seems to implies that, even in the linear theory, a positive linear growth rate $\gamma_k > 0$ is only a necessary but *not sufficient* condition for electron heat transport to occur. In addition the linear growth-rate must be larger than the threshold $\gamma_k^{\text{th}} = |\omega_k - \omega_{\text{res}}|$. In the fluid CTEM model, this threshold scales like $\gamma_k^{\text{th}} \sim 1 - \epsilon_n$. This suggests that flat density profiles $\epsilon_n \sim 1$ will lower the synchronization threshold and trigger phase-locking of the crossphase, and hence electron heat transport, while peaked density profiles $|\epsilon_n| \ll 1$ will require a higher linear growth-rate - higher η_e - to trigger electron heat transport. In analogy with the ‘phase reponse curve’ associated to oscillators with global couplings, one can define the ‘crossphase response’ curve (CPR) as the r.h.s. of Eq. (85). The phase response is plotted for a value $\zeta_k^0 = 0.2\pi$ [Fig.6]. A similar idea was introduced in Refs. [9] and [30].

Note that, for the ∇T_e -driven CTEM model, the turbulent electron heat flux can be written in the form:

$$Q_e = \sum_k k_y \frac{|\phi_k|^2}{\beta_k} \sin \zeta_k, \quad (88)$$

where $\beta_k = |\phi_k|/|s_{ek}|$ is the amplitude ratio between electron entropy fluctuations s_{ek} and potential fluctuations ϕ_k , which takes the form:

$$\beta_k = \frac{\gamma_k}{(\eta_e - \frac{2}{3})\omega_* \sin \zeta_k}, \quad (89)$$

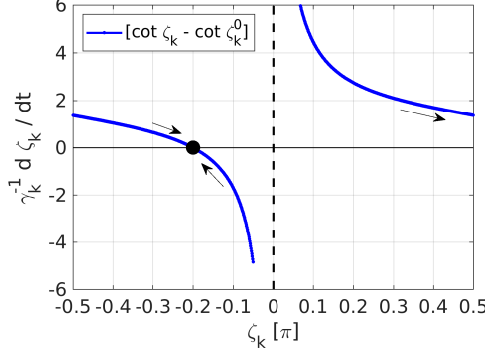


Figure 6: Phase response curve $\frac{d\zeta_k}{dt} = f(\zeta_k)$ for the ∇T_e -driven CTEM fluid model. The curve is shown for a value $\zeta_k^0 = -0.2\pi$ of the phase-locked solution.

Replacing the amplitude ratio β_k by its expression (89), this yields:

$$Q_e = \sum_k k_y \frac{(\eta_e - \frac{2}{3})\omega_*}{\gamma_k} |\phi_k|^2 \sin^2 \zeta_k \quad (90)$$

Remember that ζ_k is the *instantaneous* crossphase between s_{ek} and ϕ_k . Eq. (85) can be further linearized around the phase-locked crossphase (86). Using the Taylor series $\cot \zeta_k \simeq \cot \zeta_k^0 + \cot'(\zeta_k^0)[\zeta_k - \zeta_k^0]$, one obtains, after some algebra:

$$\frac{\partial \zeta_k}{\partial t} \simeq -\frac{1}{\tau_k}(\zeta_k - \zeta_k^0), \quad (91)$$

where τ_k is the linear response time (relaxation time) at wavenumber \mathbf{k} :

$$\tau_k = \left[(1 + \cot^2 \zeta_k^0) \gamma_k \right]^{-1}, \quad (92)$$

which is of the order of the turbulence correlation time τ_c , i.e. $\tau_k \propto \gamma_k^{-1} \sim \tau_c$, when taking into account resonance-broadening due to turbulence, i.e. $\gamma_k \rightarrow \gamma_k + D_t k_\perp^2$, with D_t the turbulent diffusivity. Note that the crossphase dynamics Eq. (91) has a similar form as the heat flux dynamics of the traffic-jam model of Ref. [31, 32]

$$\frac{\partial Q}{\partial t} = -\frac{1}{\tau}(Q - Q_0), \quad (93)$$

where $Q = \sum_k Q_k$ is the heat flux, $Q_0 = \sum_k Q_k^0$ is the mean heat flux, and τ is the response time between the instantaneous heat-flux and its relaxed value, which is also of the order of the turbulence correlation time [31, 33]. From the crossphase dynamics Eq. (91), one sees that the relaxation time becomes very large $\tau_k \rightarrow \infty$, when the system is near marginality $\gamma_k \rightarrow 0$. Hence, one expects a *slow dynamics* of the crossphase (and associated heat-flux) close to marginality, where the crossphase (and associated heat transport) can remain far from their phase-locked value (the crossphase usually assumed in quasi-linear transport codes), for a significant time.

Hence, there seems to be a connection between the ‘traffic-jam’ model of Refs. [31, 32], and the crossphase dynamics. More work needs to be done to better understand this connection.

4 Discussion and conclusions

Let us first discuss the comparison of the fluid model and the linear gyrokinetic simulations using the GKPSP code [11]. In the ITG case, the fluid model (57,58) only shows qualitative similarity with the gyrokinetic simulation. However, the ITG frequency is more closely matched to the gyrokinetic result than the growth-rate, which shows a large difference. Frequency and growth-rate were also compared with Nilsson et al. [4]. The ITG frequency from the ITG model used in this work [22] more closely matches the gyrokinetic result compared to that of Ref. [4], except for $k_y \rho_s \ll 1$. For the CTEM case also, only qualitative similarity is found between the fluid model and GKPSP simulation, except at low wavenumbers $k_y \rho_s < 0.2$. This is not surprising, since the ∇T_e -driven CTEM fluid model does not contain inertial - i.e. polarization - effects, which are stabilizing at larger wavenumbers $k_y \rho_s \sim 1$.

Let us now discuss the Kuramoto-like equation (85) describing the crossphase dynamics of the fluid CTEM model. Eq.(85) is very similar to the Kuramoto equation [29], except that the associated phase-response curve is of the form ‘cotangent’ instead of a sinusoid for the Kuramoto model. It thus has period π instead of 2π for the Kuramoto model. One particular interesting property of the Kuramoto model is the synchronization of coupled oscillators if the coupling is above a certain threshold K_{th} proportional to the entrainment frequency. By analogy, we may say that for CTEM, the transport *crossphase* - associated to electron heat transport - at different wave-numbers become

synchronized when above the threshold. For CTEM, the threshold depends on the difference between the mode frequency and the *resonance* frequency. The form of the Kuramoto-like equation (85) for the CTEM instability, which is a reactive instability is very different than the one for the collisional drift-wave instability or the weakly-dissipative trapped electron mode (DTEM) [9]. In the latter case, the cotangent function on the r.h.s. of Eq. (85) is replaced by the (negative of the) tangent function, and it is multiplied by the electron-ion collision frequency ν_{ei} instead of the linear growth-rate, since $\gamma_k \ll \nu_{ei}$ for collisional instabilities. This may partly explain the difference between the nature of the two types of instabilities.

In conclusion, the nonlinear dynamics of the ∇T_e -driven CTEM model - analyzed linearly here - will be investigated in future work, especially the zonal flows and associated zonal T_e corrugations and their impact on electron heat transport and staircase formation [12, 13, 14, 31].

Acknowledgements

The authors would like to thank Jae-Min Kwon, Sumin Yi, Sehoon Ko, P.H. Diamond, I. Dodin and X. Garbet for helpful discussions. This work was supported by R&D Program through Korean Institute of Fusion Energy (KFE) funded by the Ministry of Science and ICT of the Republic of Korea (KFE-EN2241-8).

Appendix: Validity of the ∇T_e -driven CTEM limit

Linearizing the original system (1-4) for $g_i = g_e = 1$, one obtains:

$$-i\omega n_k + if_t\omega_*\phi_k = -i\omega_{de}(n_k - f_t\phi_k + f_tT_{ek}), \quad (94)$$

$$-i\omega T_{ek} + i\eta_e\omega_*\phi_k = -\frac{2}{3f_t}i\omega_{de}(n_k - f_t\phi_k + \frac{7}{2}f_tT_{ek}), \quad (95)$$

$$-(1 - f_t + k_\perp^2)i\omega\phi_k + i(1 - f_t - \frac{1 + \eta_i}{\tau}k_\perp^2)\omega_*\phi_k =$$

$$i\omega_{de}[(1 - f_t)(1 + 1/\tau)\phi_k + T_{ik} + (1 + 1/\tau)n_k + f_tT_{ek}], \quad (96)$$

$$\begin{aligned} -i\omega T_{ik} = & i\frac{\omega_{de}}{\tau} \left[\frac{2}{3\tau}(1 - f_t + \tau)\phi_k + \frac{2}{3\tau}n_k + \frac{7}{3}T_{ik} \right] - i \left[\eta_i - \frac{2}{3\tau}(1 + \eta_i + \tau)k_\perp^2 \right] \frac{\omega_*}{\tau}\phi_k \\ & - \frac{2}{3\tau^2}ik_\perp^2\omega_{de} \left[(1 + \tau)\phi_k + \frac{\tau}{1 - f_t}T_{ik} + \frac{1 + \tau}{1 - f_t}n_k + \frac{\tau f_t}{1 - f_t}T_{ek} \right], \end{aligned} \quad (97)$$

with $\omega_* = k_y v_{*e}$ the electron diamagnetic frequency, $\omega_{de} = \epsilon_n \omega_*$ the precession-drift frequency. The linear dispersion relation is best obtained by first transforming the system. Adding Eqs. (94) and (96) yields the ion continuity equation:

$$-i\omega(n_{ik} + k_\perp^2\phi_k) + \left(1 - \frac{1 + \eta_i}{\tau}k_\perp^2\right)i\omega_*\phi_k = i\frac{\omega_{de}}{\tau} \left[(1 - f_t + \tau)\phi_k + n_k + \tau T_{ik} \right], \quad (98)$$

with, due to quasi-neutrality, $n_{ik} = n_k + (1 - f_t)\phi_k$ the ion density perturbation. This can also be written as:

$$-i\omega(n_{ik} + k_\perp^2\phi_k) + \left(1 - \frac{1 + \eta_i}{\tau}k_\perp^2\right)i\omega_*\phi_k = -i\omega_{di}(\tau\phi_k + n_{ik} + \tau T_{ik}), \quad (99)$$

with $\omega_{di} = -\omega_{de}/\tau < 0$ the ion magnetic drift.

The linear ion density response is then:

$$(\omega - \omega_{di})n_{ik} = \left[\omega_* + \tau\omega_{di} - k_\perp^2(\omega + \alpha_i\omega_*) \right] \phi_k + \tau\omega_{di}T_{ik}, \quad (100)$$

where $\alpha_i = (1 + \eta_i)/\tau$ represents ion FLR effects. Multiplying Eq. (97) by 3/2 and subtracting Eq. (99) yields the ion heat balance:

$$-i\omega \left[\frac{3}{2}T_{ik} - \frac{1 - f_t}{\tau}\phi_k - \frac{n_k}{\tau} \right] - \frac{3}{2}i(\eta_i - \frac{2}{3})\omega_*\phi_k = -\frac{5}{2}i\omega_{di}T_{ik} \quad (101)$$

The associated linear ion temperature response is:

$$T_{ik} = \frac{1}{\omega - \frac{5}{3}\omega_{di}} \left[\left(\eta_i - \frac{2}{3} \right) \omega_* \phi_k + \frac{2}{3\tau} \omega n_{ik} \right] \quad (102)$$

Replacing T_{ik} in terms of n_{ik} and ϕ_k in Eq. (100), the linear ion density response takes the form:

$$n_{ik} = \frac{(\omega_* + \omega_{di})(\omega - \frac{5}{3}\omega_{di}) - k_\perp^2(\omega + \alpha_i\omega_*)(\omega - \frac{5}{3}\omega_{di}) + (\eta_i - \frac{7}{3} + \frac{5}{3}\epsilon_n)\omega_*\omega_{di}}{N_i} \phi_k, \quad (103)$$

with $N_i = \omega^2 - \frac{10}{3}\omega_{di}\omega + \frac{5}{3}\omega_{di}^2$. Next, we analyze the linear electron dynamics. Multiplying Eq. (95) by $\frac{3}{2}f_t$ and subtracting Eq. (94), one obtains the electron heat balance:

$$-i\omega \left[\frac{3}{2}f_t T_{ek} - n_k \right] + \frac{3}{2}i f_t \left[\eta_e - \frac{2}{3} \right] \omega_* \phi_k = -\frac{5}{2}i f_t \omega_{de} T_{ek} \quad (104)$$

This yields the linear electron temperature response:

$$T_{ek} = \frac{1}{f_t(\omega - \frac{5}{3}\omega_{de})} \left[\left(\eta_e - \frac{2}{3} \right) f_t \omega_* \phi_k + \frac{2}{3} \omega n_k \right] \quad (105)$$

Expressing T_{ek} in terms of ϕ_k and n_k , the linear electron density response is then:

$$(\omega - \omega_{de})n_k = f_t(\omega_* - \omega_{de})\phi_k + \frac{\omega_{de}}{\omega - \frac{5}{3}\omega_{de}} \left[\frac{2}{3}\omega n_k + f_t \omega_* \left(\eta_e - \frac{2}{3} \right) \phi_k \right] \quad (106)$$

After some algebra, one obtains:

$$n_k = f_t \left[\omega - \omega_{de} - \frac{2}{3} \frac{\omega_{de}\omega}{\omega - \frac{5}{3}\omega_{de}} \right]^{-1} \left[\omega_* - \omega_{de} + \left(\eta_e - \frac{2}{3} \right) \frac{\omega_*\omega_{de}}{\omega - \frac{5}{3}\omega_{de}} \right] \phi_k \quad (107)$$

Note the identity $\omega_{de}(1 + \frac{5}{3}\delta) = \omega\delta$, with $\delta = \omega_{de}/(\omega - \frac{5}{3}\omega_{de})$ obtained in Ref. [34]. The denominator can be rewritten as $\omega - \frac{5}{3}\omega_{de}(1 + \frac{2}{3}\delta) = \omega - \frac{5}{3}(\omega - \omega_{de})\delta$. Then, multiplying both numerator and denominator of expression (107) by $\omega - \frac{5}{3}\omega_{de}$, one obtains - after some algebra - the following linear trapped-electron density response:

$$n_k = f_t \frac{(\omega_* - \omega_{de})(\omega - \frac{5}{3}\omega_{de}) + (\eta_e - \frac{2}{3})\omega_*\omega_{de}}{N_e} \phi_k, \quad (108)$$

with $N_e = \omega^2 - \frac{10}{3}\omega_{de}\omega + \frac{5}{3}\omega_{de}^2$. Finally, using quasi-neutrality $n_{ik} = n_k + (1 - f_t)\phi_k$ yields the following linear dispersion relation:

$$\frac{(\omega_* + \tau\omega_{di})(\omega - \frac{5}{3}\omega_{di}) - k_\perp^2\omega + (\eta_i - \frac{2}{3})\omega_*\omega_{di}}{N_i} = f_t \frac{(\omega_* - \omega_{de})(\omega - \frac{5}{3}\omega_{de}) + (\eta_e - \frac{2}{3})\omega_*\omega_{de}}{N_e} + 1 - f_t, \quad (109)$$

In the limit of pure CTEM, the mode frequency resonates with the precession-drift frequency $\omega \sim \frac{5}{3}\omega_{de}$. In this limit, $N_i \gg N_e$, i.e. $|n_{ik}| \ll (1 - f_t)|\phi_k|, |n_k|$ and the dispersion relation (109) reduces to:

$$f_t \frac{(\omega_* - \omega_{de})(\omega - \frac{5}{3}\omega_{de}) + (\eta_e - \frac{2}{3})\omega_*\omega_{de}}{N_e} + 1 - f_t \simeq 0, \quad (110)$$

References

- [1] J.C. Adam, W.M. Tang and P.H. Rutherford, *Phys. Fluids* 19, 561 (1976).
- [2] J. Weiland, Collective modes in inhomogeneous plasmas, *Kinetic and Advanced Fluid Theory, Bristol: IOP Publishing* (2000), p. 115.
- [3] H. Nordman, J. Weiland and A. Jarmen, *Nucl. Fusion* 30, 983 (1990).
- [4] J. Nilsson, M. Liljestrom and J. Weiland, *Phys. Fluids B* 2, 2568 (1990).
- [5] A. Jarmen, P. Anderson and J. Weiland, *Nucl. Fusion* 27, 941 (1987).
- [6] J. Anderson, H. Nordman, R. Singh and J. Weiland, *Plasma Phys. Control. Fusion* 48, 651 (2006).
- [7] M. Leconte and T. Kobayashi, *Phys. Plasmas* 28, 014503 (2021).
- [8] M. Sasaki, K. Itoh, B.F. McMillan, T. Kobayashi, H. Arakawa and J. Chowdhury, *Phys. Plasmas* 28, 112304 (2021).
- [9] M. Leconte and R. Singh, *Plasma Phys. Control. Fusion* 61, 095004 (2019).
- [10] C.Y. An, B. Min and C.B. Kim, *Plasma Phys. Control. Fusion* 59 (2017).
- [11] J.M. Kwon, L. Qi, S. Yi and T.S. Hahm, *Comput. Phys. Commun.* 215, 81 (2017).

- [12] G. Dif-Pradalier, G. Hornung, P. Ghendrih, Y. Sarazin, F. Clairet, L. Vermare, P.H. Diamond, J. Abiteboul, T. Cartier-Michaud, C. Ehrlacher *et al.*
- [13] G. Dif-Pradalier, G. Hornung, X. Garbet, P. Ghendrih, V. Grandgirard, G. Latu and Y. Sarazin, *Nucl. Fusion* 57, 066026 (2017).
- [14] L. Qi, M.J. Choi, M. Leconte, T.S. Hahm and J.M. Kwon, *Nucl. Fusion* 62, 126025 (2022).
- [15] J.Y. Lang, S.E. Parker and Y. Chen, *Phys. Plasmas* 15, 055907 (2008).
- [16] T.S. Hahm and W.M. Tang, *Phys. Plasmas* 3, 242 (1996).
- [17] J. Anderson and H. Nordman, *J. Plasma Phys.* 72, 609 (2006).
- [18] X. Garbet, L. Garzotti, P. Mantica, H. Nordman, M. Valovic, H. Weisen and C. Angioni, *Phys. Rev. Lett.* 91, 035001 (2003).
- [19] Y. Zhou, H. Zhu and I. Dodin, *Plasma Phys. Control. Fusion* 61, 075003 (2019).
- [20] P.H. Diamond: Lectures from UC San Diego Physics 218C , Spring 2021, Lecture 2b: <https://courses.physics.ucsd.edu/2021/Spring/physics218c/lecture.html>
- [21] X. Garbet, N. Dubuit, E. Asp. Y. Sarazin, C. Bourdelle, P. Ghendrih and G.T. Hoang, *Phys. Plasmas* 12, 082511 (2005).
- [22] J. Anderson, H. Nordman, R. Singh and J. Weiland, *Phys. Plasmas* 9, 4500 (2002).
- [23] H. Nordman, B. Jhowry and J. Weiland, *Phys. Fluids B* 05, 3465 (1993).
- [24] M. A. Beer, *PhD Thesis: Gyrofluid models of turbulent transport in tokamaks*, p.16, 1995.
- [25] Rameswar Singh and P.H. Diamond, *Plasma Phys. Control. Fusion* 63, 035015 (2021).
- [26] A. I. Smolyakov, P.H. Diamond and M.V. Medvedev, *Phys. Plasmas* 7, 3987 (2000).

- [27] W.E. Pauli, *Zeitschrift für Physik* 37, 263 (1926), https://www.en.wikipedia.org/wiki/Pauli_matrices
- [28] I.Y. Dodin, private communication
- [29] J. A. Acebron, L.L. Bonilla, J.C. Perez Vicente, F. Ritort and R. Spigler, *Rev. Mod. Phys.* 77, 137 (2005).
- [30] Z.B. Guo and P.H. Diamond, *Phys. Rev. Lett.* 100, 215003 (2015).
- [31] Y. Kosuga, P.H. Diamond, G. Dif-Pradalier and O.D. Gurcan, *Phys. Plasmas* 21, 055701 (2014).
- [32] O.D. Gurcan, P.H. Diamond, X. Garbet, V. Berionni, G. Dif-Pradalier, P. Hennequin, P. Morel, Y. Kosuga and L. Vermare, *Phys. Plasmas* 20, 022307 (2013).
- [33] L. Qi, J.M. Kwon, T.S. Hahm, S. Yi and M.J. Choi, *Nucl. Fusion* 59, 026013 (2019).
- [34] A. Jarmen and H. Nordman, *Plasma Phys. Control. Fusion* 34, (1992).